Smart Mater. Struct. 29 (2020) 095018 (11pp) - https://doi.org/10.1088/1361-665X/aba81e

Fatigue life characterization and modeling of a Ni-Ti snake-like element for mini actuation

Adelaide Nespoli (1), Francesca Berti (2), Lorenza Petrini (3), Giancarlo Pennati (2), Elena Villa (1), Francesca Passaretti (1)

(1): Consiglio Nazionale delle Ricerche – Istituto di Chimica della Materia Condensata e di Tecnologie per l'Energia (CNR_ICMATE), via G. Previati 1/e, 23900 Lecco (Italy)
(2): Politecnico di Milano, Dipartimento di Chimica, Materiali e Ingegneria Chimica, Piazza Leonardo da Vinci 32, 20133 Milano (Italy)
(3): Politecnico di Milano - Dipartimento di Ingegneria Civile e Ambientale, Piazza Leonardo da Vinci 32, 20133 Milano (Italy)

Corresponding author
Adelaide Nespoli
CNR-ICMATE, Via G. Previati 1/E, 23900 Lecco (Italy)
Phone: +39 0341 2350 116
Fax: +39 0341 2350 114
e-mail: adelaide.nespoli@cnr.it

Abstract

The interest in the design of shape memory alloy (SMA) actuators is recently broadened thanks to their high power density and versatility. In particular, snake-like Ni-Ti actuators demonstrated high potential at the mini- and micro-scales as SMA non-conventional active elements, due to their capacity to provide significant displacements in a very limited space and over a high number of thermo-mechanical cycles. In this study, the fatigue behavior of a snake-like Ni-Ti element has been investigated to identify the Wöhler F-N curve. Moreover, a validated digital twin of the device was prepared and used to evaluate the stress distribution throughout the fatigue tests, to convert the experimental data into a Wöhler stress-life curve. The numerical description of shape memory behavior was performed through the Petrini-Bertini constitutive model, which also allowed a better insight for future shape and functional optimization of the device.

Keywords

Wöhler curve, Ni-Ti actuator, snake-like shape, fatigue, Petrini-Bertini model

Smart Mater. Struct. 29 (2020) 095018 (11pp) - https://doi.org/10.1088/1361-665X/aba81e

1. Introduction

Shape memory alloys (SMA) have increased attractiveness in actuation because of their capability to promote motion through the conversion of thermal energy in mechanical work (shape memory effect, SME) [1]. The ever-increasing miniaturization of many industrial products needs for smaller and smaller actuators. According to this trend, SMA can provide an excellent alternative to traditional mini-actuators, like electric, pneumatic and hydraulic engines, thanks to their simple and noiseless mechanism, lightness, low power supply, high mechanical performances, and high power/weight ratio [2 - 6].

It is a known fact that the SMAs actuators exhibit their best functional performances at the mini- and micro-scales, with a higher power density than to the common lightweight technologies [7 - 9]. Different kinds of actuation elements have already been investigated, among which the straight wire and the helical spring are the most exploited [10 - 13]. Besides, in previous works of the authors [14 - 16], a Nickel-Titanium (Ni-Ti) snake-like actuator was manufactured and characterized, and its promising mechanical performances were proved.

Recently, Frost et al. [17] reported an interesting study on superelastic Ni-Ti snake-like springs and revealed that stress-induced martensite tends to form in a localized manner; this localization affects the distribution of phases and strains and it is suggested to be critical for failure in Ni-Ti polycrystalline structures [18].

One of the most challenging features of any SMA actuator is represented by its ability to withstand structural and functional fatigue [19, 20], because of the simultaneous thermal and mechanical cyclic inputs. These may cause damage and fracture, as well as changes in the functional response, such as strain drift at the beginning of cyclic testing, strain stabilization and accumulation of plastic deformation [16, 21]. The basics of the fatigue phenomena are related to the complexity of the martensitic transformation and the microstructure [22] of the SMA element. However, fatigue may be influenced by other several practical factors, such as i) the quality of the alloy (related to the presence and the number of defects such as titanium carbide TiC inclusions [23], the voids generated during the working process by the crush of TiC particles, the precipitates after annealing); ii) the geometry [16] and the orientation during regular functioning [24] of the SMA element; iii) the applied load and the corresponding strain; iv) the heating source parameters [25], and v) the ambient temperature compared to the characteristic transformation temperature of the material. This is much true for the snake-like design for which the repetitive bending and straightening of the curved parts causes a localized stress concentration which promotes damage as crack nucleation [16]. The optimization of the thermo-mechanical response of a snake-like SMA element needs a specific study of fatigue life. In this work, we propose an investigation of the functional fatigue of a symmetrical snake-like SMA element, which may be versatile in many engineering applications such as miniature robotics, gripping devices and, moving towards biomedical systems, smart surgical tools [26 - 28]. In particular, experimental tests were carried out

Smart Mater. Struct. 29 (2020) 095018 (11pp) - https://doi.org/10.1088/1361-665X/aba81e

to identify its behavior under different cyclic load levels to derive the corresponding Wöhler curve. In the present work, a validated finite element model of the snake-like element was devoted to mimicking the device functioning behavior through a simple and cost-effective approach, which neglects the complex micromechanical mechanisms occurring at the local level. This would be very convenient for industries interested in dealing with the preliminary design and verification phases of new prototypes.

2. Materials and methods

2.1 Thermo-mechanical behavior of SMA material

Commercial Ni-Ti wires with the chemical composition of $Ni_{49}Ti_{51}$ (at.%) and diameter of 0,2 mm were used to produce the snake-like elements. A few straight samples were produced to perform material characterization. All the specimens in both the straight and snake-like shapes were annealed at 500°C for 10 minutes to promote the shape memory effect. The snake-like element is characterized by simple geometry, consisting of four loops, identified by a progressive roman number (from I to IV) as in Figure 1a. A few geometrical quantities allow its description (referring to Figure 1a): D is the distance between the peaks of two consecutive loops, R is the curvature radius and H is the total height. The x axis represents the direction of both the applied load and the deformation during functioning.

The phase transformation temperatures of annealed samples are 48°C, 46°C and 43°C for the rhombohedral start, peak and finish temperatures (Rs, Rp, Rf), -3°C, -2°C and -16°C for the martensite start, peak and finish temperatures (Ms, Mp, Mf) and 49°C, 55°C and 60°C for the austenite start, peak and finish temperatures (As, Ap, Af) (Figure 1b).

According to the material transformation temperatures, two uniaxial tensile tests were performed on the Ni-Ti wires in the martensite and austenite phases ($T<Mf$ = -20 °C and $T>Af$ = 70 °C, respectively) through a standard tensile testing machine (Q800 TA Instruments) equipped with an environmental chamber. Moreover, two strain recovery tests (from 130 °C to -70 °C with 5°C/min heating/cooling rate at a constant stress of 150 MPa and 200 MPa), also performed on the Ni-Ti wires, were used for a full characterization of the device thermo-mechanical behavior.

Smart Mater. Struct. 29 (2020) 095018 (11pp) - https://doi.org/10.1088/1361-665X/aba81e

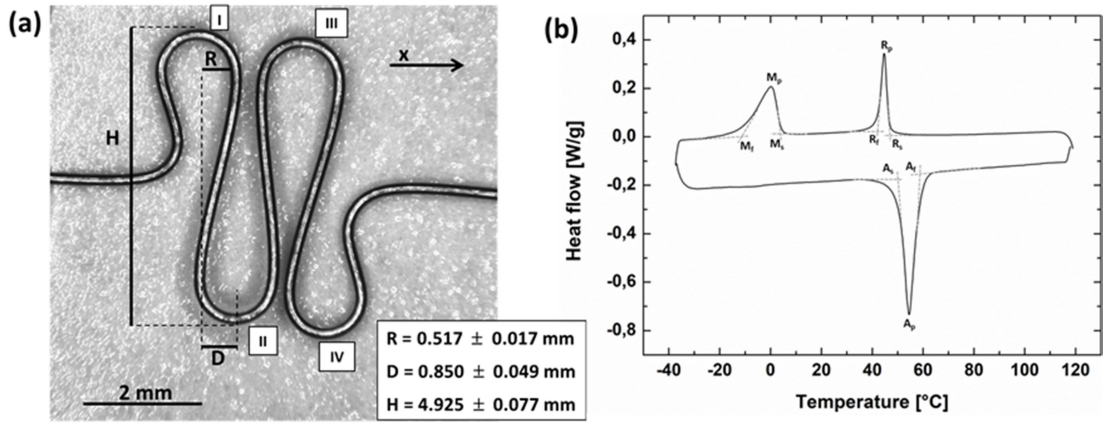

Figure 1. (a): An optical microscope image of the snake-like Ni-Ti actuator, with details of the main geometrical features and the corresponding values (obtained through measurements performed on five elements). All the loops are identified by a roman number from I to IV, from left to right. The x axis represents the direction of both the applied load and the deformation during functioning; (b): the output of the DSC analysis for the identification of the material transformation temperatures.

2.2 Study of fatigue behavior

Due to the final application of the mini actuator, it is crucial to fully characterize its response to cyclic loads. In these cases, international standards recognize the Wöhler's (or load-life or stress-life) diagram as the most effective way of presenting the fatigue results. The realization of this curve for the snake-like element was accomplished following the ISO 12107 [29]. Numerous fatigue tests, performed at different load levels, allows the registration of the corresponding maximum number of cycles that can be reached without failure (N, also known as fatigue life). This practice allows describing only that part of the Wöhler's diagram known as "finite life", where the load-life relationship may be reasonably approximated by a straight line for a specific interval of load levels. Moreover, it is possible to identify another area of the diagram, usually referred to as "infinite life", characterized by an almost constant load level, named endurance limit F_{LIM} and defining the material fatigue strength, i.e. the maximum load that can be applied without registering any failure for any N.

In this work, five different levels of load were considered for the definition of the "finite life" fatigue behavior. According to previous results [16], the snake-like element was tested under loads higher than 0.1 N, in particular, the following values were selected: 0.145 N, 0.171 N, 0.201 N, 0.294 N, 0.392 N. During tests, the actuator was free to deform as no physical limits were adopted. The reliability of test results is primarily dependent on the number of specimens tested; in the present work, referring to the ISO standard [29], a 50% failure probability with a confidence level of 90% was obtained by considering three specimens per each of load level.

A semi-log Wöhler's load-life (F-N) diagram was built after collecting these data.

Smart Mater. Struct. 29 (2020) 095018 (11pp) - https://doi.org/10.1088/1361-665X/aba81e

The Staircase method [29] was employed to estimate the endurance limit F_{LIM}. Starting from a pre-fixed load value (F_0 = 0.127 N), a sequence of failure and non-failure events was identified and collected imposing 0.003 N of load increment (ΔF). The analysis of data of the Staircase method [29] allowed the calculation of the mean value of the endurance limit, F_{LIM}, corresponding to a failure probability of 50%, and the standard deviation, STD.DEV(F_{LIM}), by the equations (1) and (2):

$$F_{LIM} = F_0 + \Delta F\left(\frac{A}{C} \pm 0.5\right) \quad (1)$$

$$STD.DEV(F_{LIM}) = 1.62\Delta F\left(\frac{CB-A^2}{C^2} + 0.029\right) \quad (2)$$

where $C = \sum f_i$, f_i is the number of the less frequent outcome at the i[th] test (i.e. force level), $A = \sum i \cdot f_i$, $B = \sum f_i \cdot i^2$. In Eq. (1), the choice of the plus or minus sign depends on the nature of the less frequent event, failure or non-failure respectively.

According to the standard, a specified number of cycles representative of the “infinite life” for the specific case, N_{LIM}, was set as run-out for the tests to perform the analysis in a reasonable time but, at the same time, being representative of the device working conditions. In this work, N_{LIM} was set to 40 000 cycles, which is compatible with the usage in the frame of mini-robotic systems and active elements for surgical tools.

In the fatigue tests, the snake-like element started from the deformed configuration induced by the load applied at ambient temperature, hence when the material was in the martensite phase: in the following this configuration is defined as deformed martensite shape. The activation by Joule effect with a 0.6 A current allowed to transform the material from martensite to austenite and reach a new configuration, in the following indicated as deformed austenite shape. During the tests, the actuator was cyclically heated for a time t_h (heating phase) and cooled for a time t_c (cooling phase) alternatively assuming the deformed austenite and martensite configurations.

Prior to the fatigue tests, an optimization of t_h and t_c were carried out to avoid early ruptures of the element due to an excess of heating during the recovery and to undue plastic accumulation during the reset step on cooling. The control of the cooling time was also helpful in limiting the drift of the strokes at the beginning of the cyclic tests and to consequently generate a stable response. To account for these features, at each applied load the cyclic response was subdivided into two portions, each characterized by a proper pair of heating and cooling times. The first pair ($t_{h,trans}$, $t_{c,trans}$) refers to the initial transient part of the cyclic response where drift occurs. The second couple ($t_{h,stab}$, $t_{c,stab}$) refers to the following stabilized response where a constant functioning is observed. According to experiments accomplished on similar geometries [16], it was assumed a stabilized response starting from the 1000[th] activation cycle, independently from the applied load. Consequently, for each of the considered loads of the fatigue test, the functioning times were identified according to the following procedure:

Smart Mater. Struct. 29 (2020) 095018 (11pp) - https://doi.org/10.1088/1361-665X/aba81e

i. the sample is thermal cycled ten times with a functioning time (t_h + t_c) defined on the base of experimental evidence and long enough to recover all the deformation (excluded the elastic deformation due to the applied load) when heated up to the austenite finishing temperature and to complete the resetting of the deformation in cooling. Using the acquired stroke-time graph at the 10^{th} cycle, $t_{h,trans}$ and $t_{c,trans}$ are identified. In particular, $t_{h,trans}$ is recognized as the portion of t_h limited by the intersection time at which the heating tangent crosses the recovery plateau; on the other hand, $t_{c,trans}$ is the part of t_c delimited by the starting point of t_c itself and the intersection time at which the cooling tangent crosses the reset plateau, as schematized in Figure 2. It is worth noting that the reset curve is smoothed due to the absence of an externally imposed cooling; therefore, the cutting off of the cooling time prevents the complete deformation of the snake-like element when in martensite phase and it allows for a reduction of the stroke.

ii. a new sample is then thermal cycled 1001 times, using $t_{h,trans}$ and $t_{c,trans}$ as heating and cooling times, respectively;

iii. the acquired stroke-time graph of the 1001^{th} cycle is used to identify the second set of functioning times ($t_{h,stab}$, $t_{c,stab}$) using the same method as for step i.

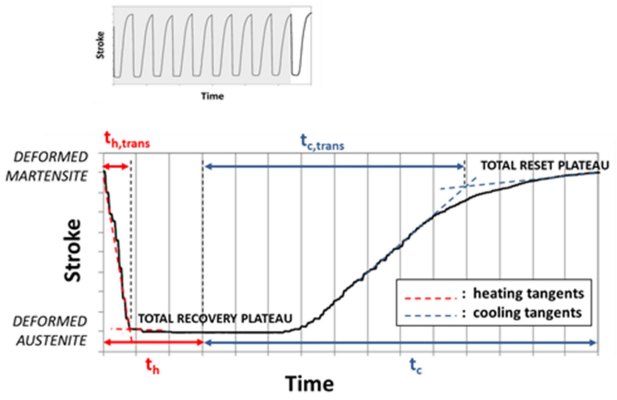

Figure 2. Schematization of the method used to determine the functioning times during the transient part of the cyclic test.

At each considered load, the described procedure allows the identification of the functioning times during the transition period $\Delta t_{trans} = t_{h,trans} + t_{c,trans}$ and during the stabilized period $\Delta t_{stab} = t_{h,stab} + t_{c,stab}$.

The stroke length of the samples (i.e. the difference between the length of the element under a specific load at the end of the cooling and heating phases) during the fatigue tests at room temperature (19 ± 1 °C) was monitored by a linear variable displacement transducer (LVDT, DC50

Smart Mater. Struct. 29 (2020) 095018 (11pp) - https://doi.org/10.1088/1361-665X/aba81e

Solartron Metrology), and Labview software was used to collect data during the measurements. When a fracture occurred, its location was registered.

2.3 FE model

The mechanical behavior of the virtual device was simulated in Abaqus 2018 (Dassault Sistémes SIMULIA Corp., Providence, RI) through a material user subroutine (UMAT). In particular, the UMAT refers to a three-dimensional phenomenological model able to describe the main properties of shape memory alloys (details about the model formulation are given in [30, 31]), including the pseudo-elasticity and the shape memory effect.

To identify the material model parameters of the austenitic and martensitic phase, the results of the thermo-mechanical tests of uniaxial tension and strain-recovery on the Ni-Ti wires were used. In particular, a simple finite element (FE) model with a unit size cubic element, meshed with a fully integrated solid element, was used to numerically reproduce the stress-strain-temperature curves of the wires.

Furthermore, the global response of the device was evaluated by experiments in which three snake-like elements were subjected to a uniaxial tensile test in force control, applied along the longitudinal axis of the element, at room temperature (19 $\pm$ 1 °C). The experiment was numerically reproduced, to verify the FE model ability to correctly describe the global behavior of the device. To minimize the computational time, the model of the snake-like actuator was reduced by exploiting an existing transverse symmetry, and the three-dimensional geometry was finally discretized with 23424 8-nodes solid elements with an incompatible mode formulation (32 elements in the halved wire cross-section).

The numerical model was then used to replicate the fatigue tests at different load levels. The maximum and minimum elongations (reached during the heating and cooling phases of the thermal cycle) were used to calculate the virtual stroke, which was compared to the average of the first five cycles during two experiments performed at the 0.145 N and 0.392 N load levels (namely, the minimum and maximum values leading to the device failure).

Knowing the local value of the stress at each location of the actuator, it was possible to recognize the most loaded location, and plot a Wöhler stress-life diagram, using the von Mises amplitude stress ($\sigma^{VM,a}$), calculated as the difference between the von Mises stress found at the end of the heating and cooling phases, respectively.

3. Results

3.1 Thermo-mechanical behavior of the SMA material

The results of the thermo-mechanical characterization of the Ni-Ti wires are shown in Figure 3. In the images, the results of the finite element analysis (FEA) have been superimposed to the experimental ones and it will be discussed in Section 3.3. Referring to the uniaxial tensile tests

Smart Mater. Struct. 29 (2020) 095018 (11pp) - https://doi.org/10.1088/1361-665X/aba81e

(Figure 3a and Figure 3b), at low temperature, i.e. in martensite state, the material has an apparent Young's modulus of 10,6 GPa and detwinning is located at 150 MPa. At high temperature (in austenite state) the material has an apparent Young's modulus of 40 GPa and the stress-induced martensite plateau is located at 400 MPa. It can be observed that in the austenite phase, the wire does not show the characteristic flag-shaped pseudoelastic curve. This is primarily ascribed to the choice of the annealing temperature which weakens the material and avoids the complete recovery of the original undeformed configuration (see the unloading of the experimental curve in Figure 3b). Despite this, the Ni-Ti wire shows good strain recovery results, as reported in Figure 3c and Figure 3d. The material shows near 8% and 8.5% recovered strain with 0.5% and 1% of residual plastic deformation, respectively at 150 MPa and 200 MPa.

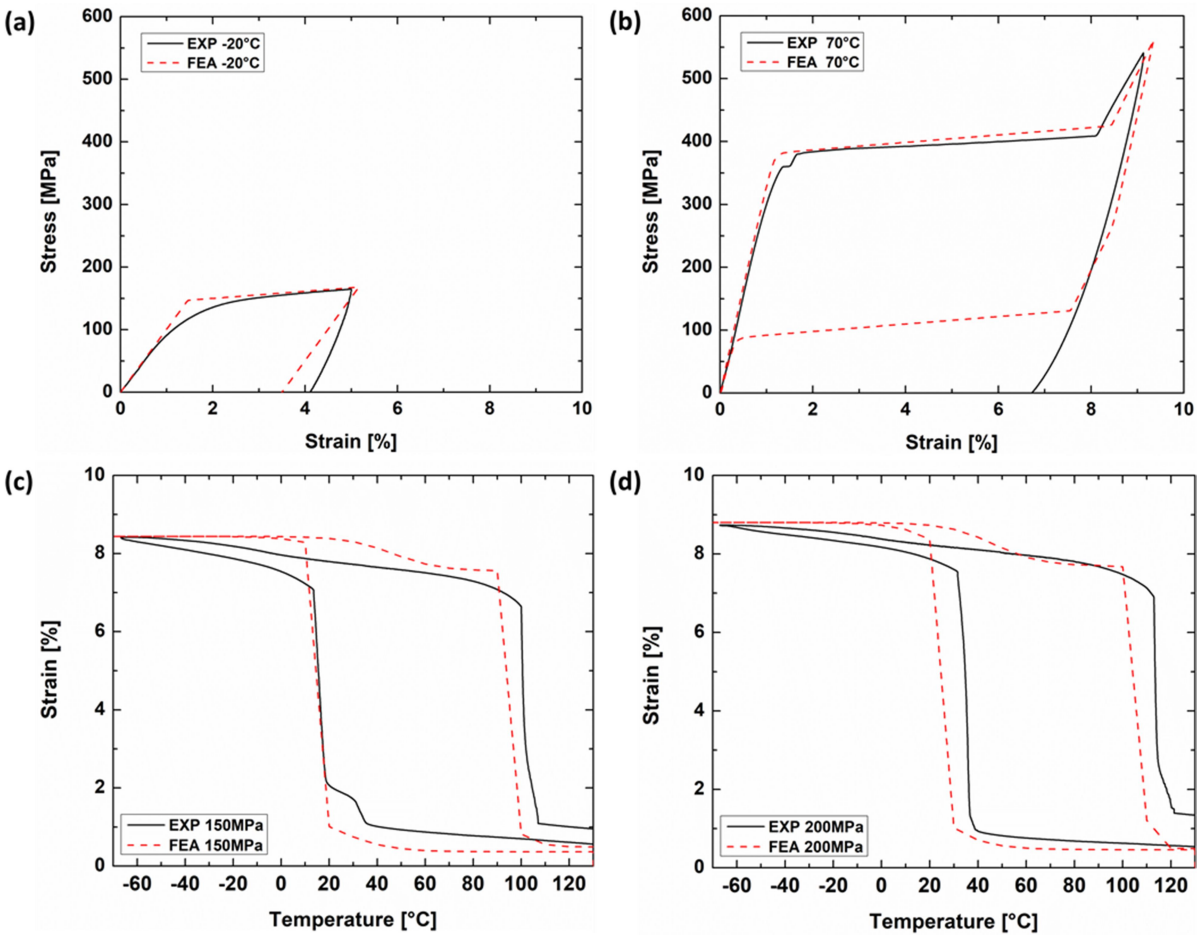

Figure 3. Comparison between experimental (EXP) and numerical (FEA) curves obtained through tests on Ni-Ti wires annealed at 500°C for 10 minutes (water quenched). (a) and (b): uniaxial tensile tests at different temperatures; (c) and (d): strain recovery tests at 150 MPa and 200 MPa.

Smart Mater. Struct. 29 (2020) 095018 (11pp) - https://doi.org/10.1088/1361-665X/aba81e

3.2 Study of fatigue behavior

The first step of the snake element fatigue life characterization was the determination of the actuation times associated with a given load. According to the procedure reported in Section 2, two functioning times were found for each load, Δt_{trans} and Δt_{stab}, which respectively characterize the transient and the stabilized behavior during the actuation.

From graphs of Figure 4a, two main behaviors are worth to be highlighted. First, it can be observed that times change with load: this happens because load prevents the complete recovery during heating and at the same time it facilitates the deformation during cooling. In addition, this trend is also promoted by an increase of the phase transformation temperatures with the applied load (Clausius-Clapeyron law): the increasing of austenite temperature with load promotes an increase of heating times, while the increasing of martensite temperature allows for a faster reset. These effects are more evident until a 0.3 N load threshold, beyond which a stabilized trend was found. Secondly, it is possible to notice a reduction in the times between the transient and the stabilized response, with particular evidence during cooling (Figure 4a). These behaviors directly affect the functioning times (Δt_{trans} and Δt_{stab}) which decreases with the load as reported in Figure 4b.

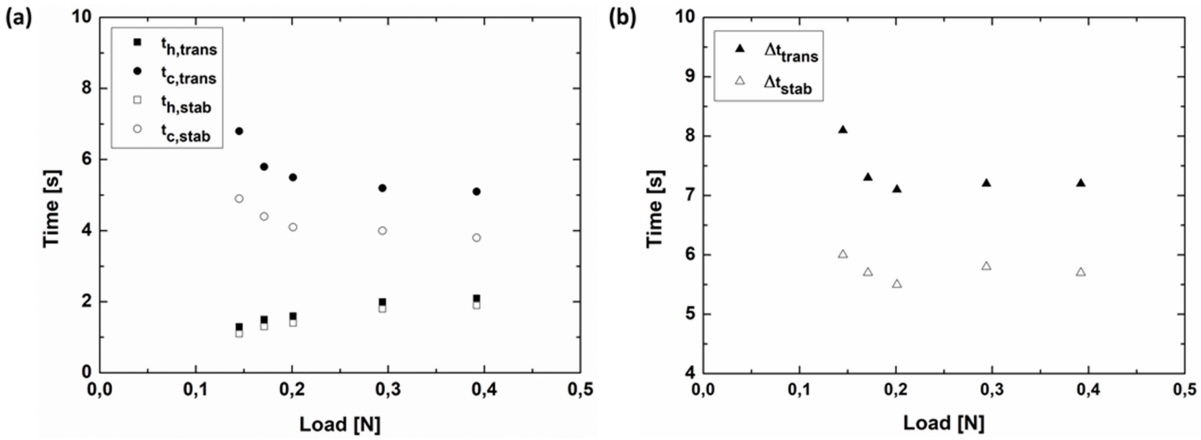

Figure 4. Times in the transient and stabilized phases of the thermo-mechanical cycling of the snake-like element. (a): transient and stabilized times during heating and cooling; (b): actuation times of a cycle in the transient and stabilized phase.

To build the “finite life” curve in the Wöhler’s diagram, the fatigue life corresponding to the three specimens tested at each load level are reported in Table 1. These data identify a cluster of points in the semi-log F-N plane that are simplified by the linear interpolation represented in Eq. (3). The majority of the fractures (10 out of 15) occurred at the same location, which is the loop identified by number III as indicated in Figure 1a; in the other cases, 4 were detected at loop number II and only 1 was located at loop number I.

Smart Mater. Struct. 29 (2020) 095018 (11pp) - https://doi.org/10.1088/1361-665X/aba81e

Table 1. Fatigue life N at a given load level F (three specimens per load level) and the corresponding fracture location (in terms of the loop number).

	Number of cycles to failure, N		
F [N]	**1st sample (location)**	**2nd sample (location)**	**3rd sample (location)**
0.145	12421(III)	34215(III)	17231(III)
0.171	17298(III)	30132(II)	16132(III)
0.201	11808(I)	16443(II)	20609(III)
0.294	10806(III)	11569(III)	9494(II)
0.392	7673(II)	9267(III)	10702(III)

$$\log(N) = 4.52 - 1.49F \quad (3)$$

The sequence of failure and non-failure events needed by the Staircase method are collected in Table 2. At the end of the fatigue campaign, there were 6 failures and 7 non-failure. The failure event is, therefore, the one considered in the analysis as the less frequent outcome.
The analysis of the Staircase data was performed on the results of 0.132 and 0.135 N load levels: in particular, referring to level 0 (0.132 N), two failures were detected while considering the first level (0.135 N), four failures were recorded. A, B and C parameters were identified from the knowledge of these data.
Solving Eq. (1) and Eq. (2), it resulted: F_{LIM} = 0,131 N and STD.DEV(F_{LIM}) = 0,001 N.

Table 2. The sequence of test outcomes following the Staircase method for the assessment of F_{LIM}.

load [N]	Specimen														
	1	2	3	4	5	6	7	8	9	10	11	12	13	14	15
0.135				X				X				X		X	
0.132			O		X		O		X		O		O		O
0.129		O*				O				O					
0.127	O*														

X: failure
O: non-failure
*not counted [29]

The semi-log Wöhler F-N diagram of the snake-like element is reported in Figure 5. An increase in the external load produced a rapid decrease in the fatigue life of the snake-like element. A scattering of the results at low forces, which can be expected in the proximity of the fatigue strength limit, is also observable.

Smart Mater. Struct. 29 (2020) 095018 (11pp) - https://doi.org/10.1088/1361-665X/aba81e

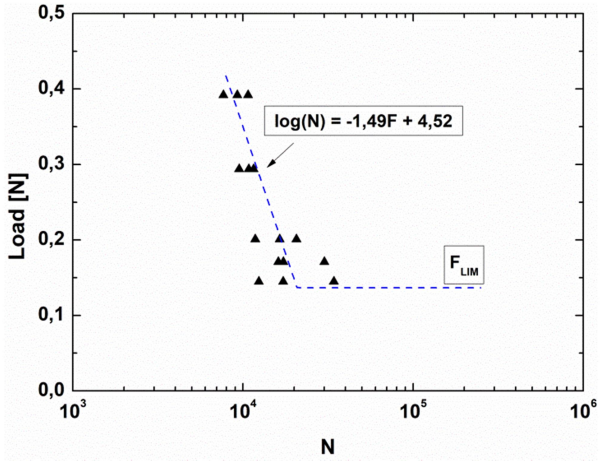

Figure 5. A semi-log Wöhler F-N diagram of the snake-like Ni-Ti element.

3.3 FE model

The results of the thermo-mechanical tests allowed a good calibration of the material model parameters, which are shown in Table 3.

Table 3. Input parameters of the material constitutive model referred to Ni-Ti wires thermal treated at 500°C for 10 minutes (water quenched). E_A: apparent Young's modulus at high temperatures; E_M: apparent Young's modulus at low temperatures; v: Poisson's ratio; ε_L: maximum transformation strain; β: Clausius Clapeyron coefficient; h_1: slope of the transformation plateau; R: elastic domain radius.

E_A [MPa]	E_M [MPa]	v [-]	ε_L [-]	β [MPa/°C]	h_1 [MPa]	R [MPa]
40000	10600	0.35	0.088	3.91	401	120

The model is representative of the thermo-mechanical behavior of the material. Its pseudoelastic curve exhibited a difference compared to the corresponding experimental curve (Figure 3b). In particular, the reverse transformation plateau (from stress-induced martensite back to austenite) could be appreciated in the numerical output whilst it was not present in the experiments. However, the model was able to catch the strain recovery curves, which determine the mini actuator's behavior (Figures 3c and 3d).

The comparison between the experimental and numerical curves related to the uniaxial tensile test on the snake-like elements highlighted a good ability of the model to catch the macroscopical behavior (Figure 6). The relative error between the experimental and numerical displacement values at different applied forces never overcame 3%.

Smart Mater. Struct. 29 (2020) 095018 (11pp) - https://doi.org/10.1088/1361-665X/aba81e

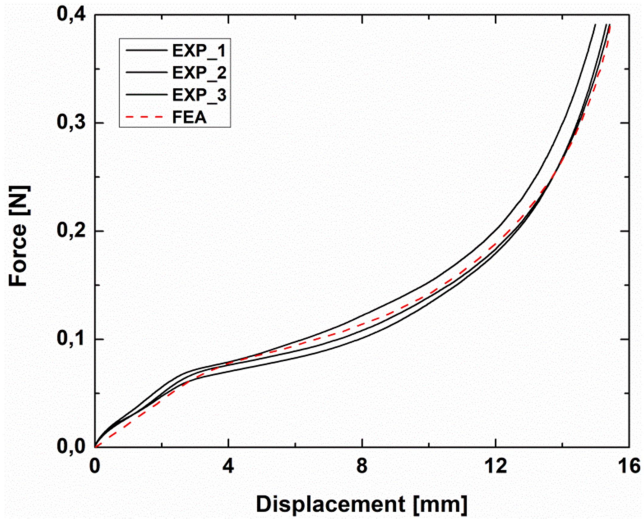

Figure 6. Comparison between the experimental (EXP) and numerical (FEA) results of the snake-like elements under tensile tests, in terms of force *vs.* displacement.

Figure 7 depicts the comparison between the numerical and experimental results of the element functioning under 0.145 N load. The numerical initial undeformed configuration (represented by the rest length L_0, Figure 7a and 7c, in black) is superimposed to the deformed martensite and austenite shapes reached at the end of the cooling (L_1, Figure 7a) and heating (L_2, Figure 7c) phases, respectively. The two photographs in Figure 7b and 7d show the corresponding configuration during the experiments. It can be observed that the load allows for a high elongation of the element due to the stretching of the loops; the stresses are mainly concentrated at the loops while the linear segments show negligible values. Table 4 reports the experimental and numerical strokes (calculated as $L_1 - L_2$), confirming a good match between the model and the experiments. as a function of the applied load for the selected cases.

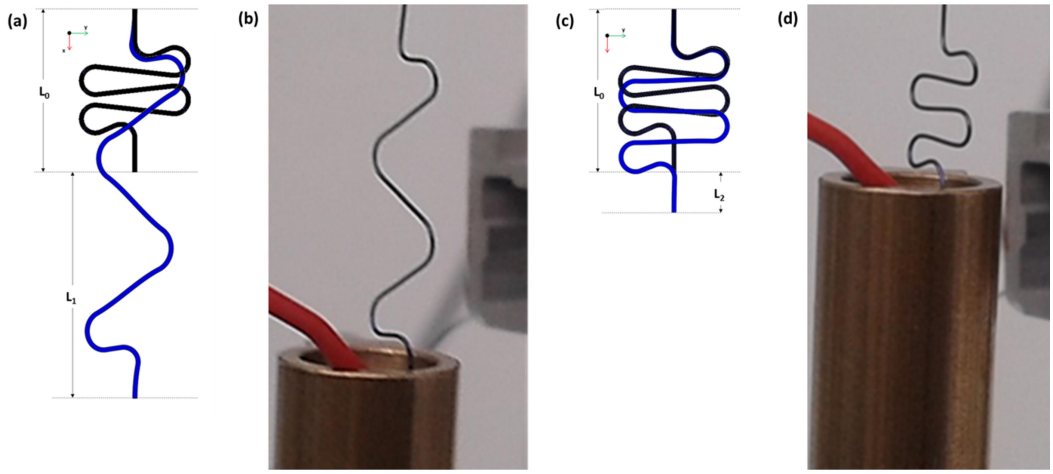

Figure 7. Experimental and numerical visualization of the actuation stroke under a load of 0.145 N. (a) The numerical elongation at the end of the cooling (in blue), defined by L_1, superimposed to the

Smart Mater. Struct. 29 (2020) 095018 (11pp) - https://doi.org/10.1088/1361-665X/aba81e

initial undeformed configuration, L_0 (in black); (b) the corresponding experimental configuration; (c) the numerical elongation at the end of the heating (in blue), defined by L_2, superimposed to the initial undeformed configuration, L_0 (in black); (d) the corresponding experimental configuration.

Table 4. Experimental and numerical strokes of the actuator as a function of the applied load in the cases of 0.145 N and 0.392 N. Experimental values are calculated as the average of the stroke happening in the first five actuation cycles of the same device.

Force [N]	Stroke EXP [mm]	Stroke FEA [mm]	Error [%]
0.145	8.24	8.29	0.61
0.392	6.31	5.98	5.23

Figure 8 reports the maximum principal stress plot at the end of the cooling and heating steps of the simulation with an applied force of 0.145 N. Loops number II and III result the most stressed ones. As shown in the boxes, the most stressed points are in the middle section of the loop (Sect. A) on the inner surface. A micrograph of the fracture surface of the loop number III of one of the snake-like elements, taken by a scanning electron microscope (W-SEM LEO 1430), is presented (Figure 8c). On the inner surface, it can be seen the nucleation site from which striations due to crack propagation depart. Hence, the simulations correctly catch the most critical area for fracture.

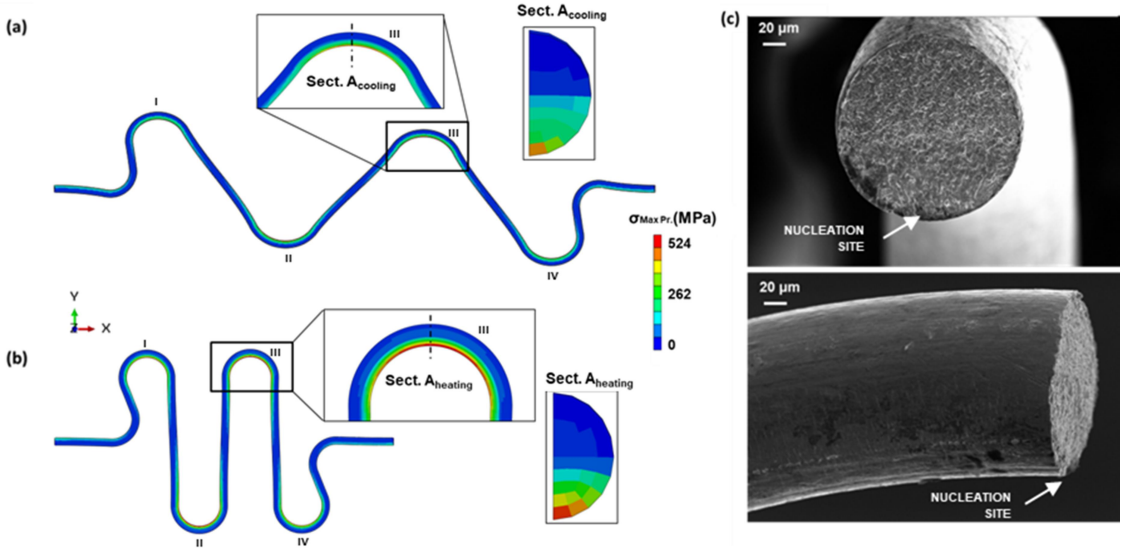

Figure 8. Distribution of the maximum principal stress in the snake-like element loaded at 0.145 N at the end of the cooling (a), and heating (b) phases; (c): SEM images of the fracture surface of a snake-like element, corresponding to Sect. A of the numerical model.

The highest stress value was assessed as 474 MPa at the end of cooling and 5

Smart Mater. Struct. 29 (2020) 095018 (11pp) - https://doi.org/10.1088/1361-665X/aba81e

4 MPa at the end of the heating phase (under F = 0.145 N). However, these values are representative of a small portion of the actuator, whilst the majority of the loops exhibits a stress value of about 250 MPa.

Following the common literature regarding the fatigue behavior of metals, the evaluation of the variation of the von Mises stress between the two phases of the thermal cycle allowed to obtain a Wöhler $\sigma^{VM,a}$-N diagram of the snake-like Ni-Ti element, see Figure 9. It can be observed that the working alternate stress limit can be assessed approximately about 150 MPa, confirming the element's ability to withstand significant stress levels.

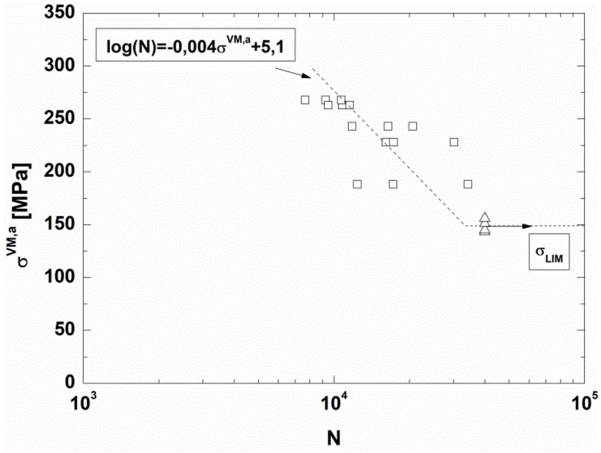

Figure 9. Semi-log Wöhler $\sigma^{VM,a}$-N diagram of the snake-like element.

4. Discussions

The main challenging feature of any SMA element to be employed as an actuator is the design of ad-hoc fatigue life, compatible with the final application. In this work, a SMA element with a novel snake-like design has been investigated to evaluate its fatigue performances.

The Wöhler $\sigma^{VM,a}$-N curve was evaluated by exploiting a numerical model, properly calibrated and validated. Experimental tests were accomplished following a standardized method, while the simulations were based on the calibration of the Petrini-Bertini model [27] for simulating the shape memory effect.

As concerns the experimental analysis, it is worth noting that the performed cutting off of both the heating and cooling times allows for faster actuation and brings some advantages. First, limiting the heating time allows controlling the maximum temperature reached during the tests, avoiding the related risk of damage. However, according to the tangent method (Figure 2), the cut of the heating time assures that the specimen recover almost completely the deformed austenite shape. As regards cooling, the limitation of time truncates the deformation of martensite, limiting the possibility to face inelastic phenomena [18] and preserving the material from structural failure.

Smart Mater. Struct. 29 (2020) 095018 (11pp) - https://doi.org/10.1088/1361-665X/aba81e

In Figure 10 where the stroke vs cycles plots for different loading conditions are reported, it is possible to notice that there is not a significant variation of the stroke during cycles: the maximum of the stroke (corresponding to the reaching of deformed martensite shape) is almost constant and variations of no more than 0.7 mm are shown at the minimum of the stroke (corresponding to the reaching of deformed austenite shape). These results show that the performed study on the actuation times positively affects the stroke length, avoiding the development of inelastic phenomena and hence preserving the material from structural failure.

This promotes a stable stroke over cycling which permits to calibrate the numerical model only considering the first five mechanical cycles. Furthermore, the need to define two sets of function times (transient and stabilized) is principally ascribed to microstructural changes that are stabilized over cycling: it is expected that the dissolution of interfaces and the formation and stabilization of some martensite variants facilitate the direct and reverse transformation by increasing Ms and decreasing As, therefore less energy is necessary for transformation [32].

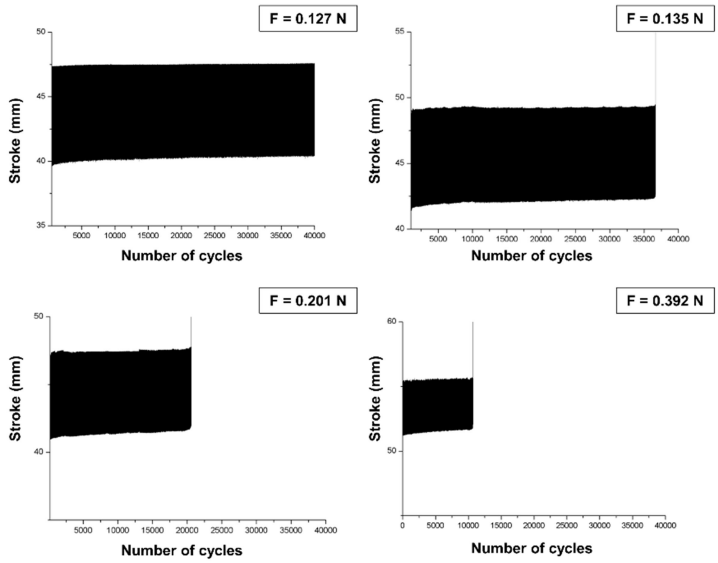

Figure 10. Stroke vs. the number of cycles during cyclic tests under different load levels, applying the heating and cooling time limitation.

The choice of the snake-like design allows manufacturing a planar element that can exhibit high strokes if compared to the straight wire but guaranteeing a reduced planar encumbrance if compared with the common spring design.

This particular feature is driven by the deformation fashion of the element during the thermal cycles. Indeed, the deformation mode of the device is dominated by the bending of the loops, which happens together with a rigid translation of the straight portions along the load direction. Under load, the snake-like element reaches stretched configuration during the cooling phase: the bending action due to the applied load is defined, for example in the case of loop III, by the

Smart Mater. Struct. 29 (2020) 095018 (11pp) - https://doi.org/10.1088/1361-665X/aba81e

distance b_1, as it is shown in Figure 11a. When heated, part of the deformation is recovered with an increase in the local stress in the loops, which is caused by the increase in the distance b_2 between the applied load and the loops themselves. It implies that, differently from a wire actuator, the stress induced in the snake-like element changes between cooling and heating, making more complex its design. Moreover, an increase in the applied load does not linearly affect the relative difference between the values of b_1 and b_2. This difference is almost constant for low values of the applied force (b_2-b_1 is 0.64 mm in the cases of 0.127 and 0.129 N, 0.67 mm in the cases of 0.132 and 0.135 N,); then it increases up to a maximum value in the case of 0.201 N (b_2-b_1=0.91 mm) for decreasing again when the maximum load 0.392 N is applied (b_2-b_1=0.67 mm).

It is interesting to notice that the b_2-b_1 value is maximum for loop II and III central loops of the element). This higher difference between the two configurations is responsible for the identification of the highest amplitude stress at these locations of the numerical model: accordingly, herein the device failure is expected. These considerations are supported by the experimental outcomes, showing 14 out of the 15 failures happening in loop II and III.

From these results, the 0.201 N load level represents a threshold above which the snake-like element exhibits lower changes between the deformed martensite and austenite configurations. This aspect might be one of the concurrent phenomena influencing the slight increase in heating times with the load increment and the decrease in cooling times (Figure 4a). Together with the geometry, the effect of gravity obstacles the complete recovery during heating and, at the same time, it promotes the deformation during cooling. Consequently, during heating, the material needed more time to recover the deformed austenite shape and less time to reach the deformed martensite with the increase of load. In addition to this, the increase of the phase transformation temperatures with the applied load (Clausius-Clapeyron law) affects in different ways the heating and cooling times: an increase in the austenite temperature with load promotes dilatation of the heating times, while the increase of the martensite temperature allows for a faster reset. This is related to the drifting of the phase transformation temperatures toward higher values during cycling that is chiefly due to dislocation built up and defects redistribution that creates internal stress in the material [34]. As a consequence, the functioning times (Δt_{trans} and Δt_{stab}) are directly affected by the aforementioned behaviors.

Due to bending, the loops are characterized by a stress distribution with high gradients, where the maximum values in tension and compression are located at the inner and outer surfaces, respectively. Figure 11b,c shows a comparison between the local stress distribution in loop III in the case of applied 0.135 N (belonging to the “infinite life” portion of the diagram) and 0.392 N (“finite life”). In the first case, there are few elements in the loop whose stresses are out of the linear elastic response (which can be assessed up to 250 MPa in martensite at room temperature of about 19°C, higher in austenite during heating), while in the second case the majority of the elements overcame these thresholds, probably entering the material plateau. The increase in the

Smart Mater. Struct. 29 (2020) 095018 (11pp) - https://doi.org/10.1088/1361-665X/aba81e

local stress leads to dramatic effects such as the reduction in fatigue life and the impossibility to gain high stroke lengths (5.98 mm in the case of 0.392 N compared to 7.83 mm of the 0.135 N). For these reasons, it is crucial to understand the optimal working conditions for a specific actuator, so that the design phase can be driven toward shape and functional optimization.

The snake-like element undergoes high stresses, about 500 MPa at some very localized areas, namely small portions of each loop when loaded lower than 0.201 N; on the other hand, when dealing with 0.294 N and 0.392 N, the almost totality of the loops cross-section bears critical stresses. Looking at Table 1 and Figure 5, it is possible to appreciate a reduction in fatigue life in these last two cases, compared to more dispersed data from the 0.145 N, 0.171 N, and 0.201 N cases. Moreover, no failure was detected in the load cases lower than 0.132 N, corresponding to stress values in the loops assessed as lower than 250 MPa. These findings are in agreement with the results shown in [33], where cycling at high stress values was demonstrated as the causes accumulation of inelastic strains, dramatically affecting the fatigue performances and the recoverable strains of a SMA actuator.

For this reason, the 500 MPa threshold should be recognized as an important design constraint for avoiding early failure in the actuators.

The numerical model herein employed is not formulated to account for those inelastic phenomena related to the micromechanics of the material. As reported in [33], phenomenological models should account for additional internal variables to catch the local changes of microstructure that affects the coupling between phase transformation and plasticity. However, the model in its form can be exploited to evaluate whether critical stress values are found in the snake-like element under each loading condition, to make the first guess on the expected issue related to early fatigue failure.

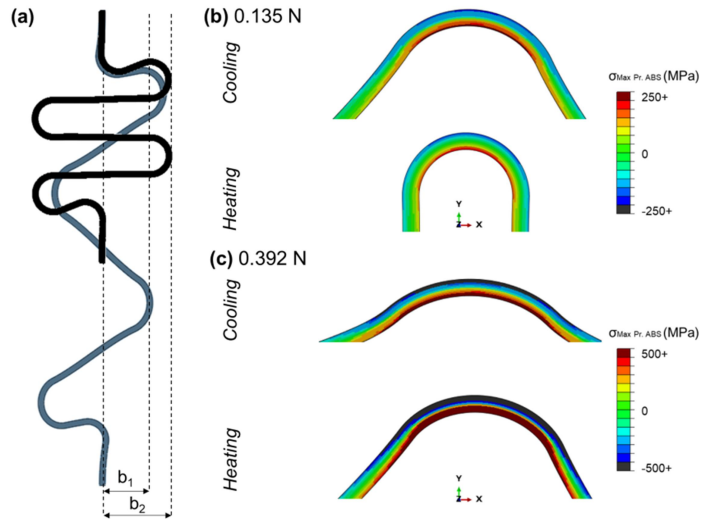

Figure 11. (a) A comparison between the deformed configuration during cooling and heating phases and the corresponding bending distances b_1 and b_2; maximum principal stresses value

Smart Mater. Struct. 29 (2020) 095018 (11pp) - https://doi.org/10.1088/1361-665X/aba81e

during the cooling and heating phases of the thermal cycle located at loop number III of the snake-like element loaded under (b) 0.135 N and (c) 0.392 N.

Finally, the Petrini-Bertini model, in its present form, does not allow to capture the tension-compression asymmetry characterizing Ni-Ti alloys. The authors are aware that this represents a limitation that might influence the local response in terms of the magnitude of the local stress and strain fields. In the future, efforts shall be spent on the upgrade of the Petrini-Bertini formulation to account for the material asymmetry.

Conclusions

In this work, a novel design of a snake-like SMA element for mini actuation, which can exhibit high strokes but guaranteeing a reduced planar layout, was investigated. Particular attention was paid at its fatigue characterization, given the interest to employ this device in the common practice. The need for controlled fatigue performances drove towards a careful study of the actuation times, whose choice greatly influences either drift-related effects during cycles or the reduction in the stroke. A validated numerical model was prepared to support the interpretation of the results, allowing the quantification of local stress and strain fields.

This study highlighted the complex deformation mechanism of the device, which is dependent on the cyclic geometrical modification which affects the maximum bearable load and, hence, the local stress value. The numerical model provides an extremely useful tool for the future optimization of the element according to the specific application.

Declaration of competing interest

The authors declare that they have no known competing financial interests or personal relationships that could have appeared to influence the work reported in this paper.

Acknowledgments

The authors gratefully acknowledge the contribution of Ilaria Giorgio, MEng for her help in the preliminary tests.

Smart Mater. Struct. 29 (2020) 095018 (11pp) - https://doi.org/10.1088/1361-665X/aba81e

References

[1] Jani JM, Leary M, Subic A, Gibson MA 2014 *Mater. Design.* **56** 1078–1113.

[2] Nematollahi M, Baghbaderani KS, Amerinatanzi A, Zamanian H, Elahinia M 2019 *Bioengineering (Basel)* **6(2)** 37.

[3] Park HB, Kim DR, Kim HJ, Wang W, Han MW, Ahn SH 2020 *Int. J. Precis. Eng. Manuf.* **21** 249–256.

[4] Sobrinho JMB, Filho FMF, Emiliavaca A, Cunha MF, Souto CR, Silva SA, Ries A 2020 *Sensors and Actuators A* **302** 111823.

[5] Eschen K, Granberry R, Abel J 2020 *Smart Mater. Struct.* **29** 035036.

[6] Megnin C, Moradi B, Zuern J, Ossmer H, Gueltig M, Kohl M 2020 *Microsystem Technologies* **26** 793–800.

[7] An L, Huang WM, Fu YQ, Guo NQ 2008 *Mater. Design.* **29** 1432-1437.

[8] Duerig TW, Melton KN, Stockel D, Wayman CM 1990 *Engineering aspects of shape memory alloys* (Butterworth-Heinemann Ltd).

[9] Mehrabi H, Aminzahed I 2020 *Microsystem Technologies* **26** 531–536.

[10] Nespoli A, Besseghini S, Pittaccio S, Villa E, Viscuso S 2010 *Sens. Actuator A* **158** 149–160.

[11] Copaci DS, Blanco D, Martin-Clemente A, Moreno L 2020 *Intern. J. Adv. Robotic Sys.* 1–15.

[12] Lu Y, Xie Z, Wang J, Yue H, Wu M, Liu Y 2019 *Intern. J. Mech. Sci.* **159** 74-80.

[13] Motzki P, Gorges T, Kappel M, Schmidt M, Rizzello G, Seelecke S 2018 *Smart Mater. Struct.* **27** 075047.

[14] Nespoli A, Bassani E, Besseghini S, Villa E 2010 *Physics Procedia* **10** 182-188.

[15] Nespoli A, Villa E, Besseghini S 2012 *J. Therm. Anal. Calorim.***109** 39-47.

Smart Mater. Struct. 29 (2020) 095018 (11pp) - https://doi.org/10.1088/1361-665X/aba81e

[16] Nespoli A, Villa E, Passaretti F 2015 *Mater. Int.* **21** 504–510.

[17] Frost M, Sedlak P, Heller L, Kaderavek L, Sittner P 2018 *Smart Mater. Struct.* **27** 095005.

[18] Chen Y, Tyc O, Molnarova O, Heller L, Sittner P 2019 *Shape Mem. Superelasticity* **5** 42-62.

[19] Mahtabi MJ, Shamsaei N, Mitchell MR 2015 *J. Mech. Behavior Biomed. Mater.* **50** 228–254.

[20] Scirè Mammano G, Dragoni E 2014 *Intern. J. Fatigue* **69** 71–83.

[21] Eggeler G, Hornbogen E, Yawny A, Wagner M 2004 *Mater. Sci. Eng. A* 24-33.

[22] Gall K, Tyber J, Wilkesanders G, Robertson SW, Ritchie RO, Maier HJ 2008 *Mater. Sci. Eng. A* **486** 389–403.

[23] Rahim M, Frenzel J, Frotscher M, Pfetzing-Micklich J, Steegmüller R, Wohlschlögel M, Mughrabi H, Eggeler G 2013 *Acta Mater.* **61** 3667–3686.

[24] Zanotti C, Giuliani P, Arnaboldi S, Tuissi A 2011 *Proc. SMST-2010 Global Solutions for Future Applications*, p.688, Springer, New York

[25] Casati R, Vedani M, Gialanella S, Tuissi A 2014 *J. Mater. Eng. Perf.* **23** 2487-2490.

[26] Sreekumar M, Nagarajan T, Singaperumal M, Zoppi M, Molfino R 2007 *Industrial Robots: An international journal* **34** 285-294.

[27] Llewellyn-Evans H, Griffiths CA, Fahmy AA 2020 *Eng. Res. Express* **2** 015027 2.

[28] Haga Y, Mineta T, Makishi W, Matsunaga T, Esashi M 2010 *Shape Memory Alloys* (ed. Sciyo).

[29] ISO12107, Analysis of Wire Position and Operating Conditions on Functioning of NiTi Wires for Shape Memory Actuators, 2003.

[30] Petrini L, Bertini A 2020 *Intern. J. Plasticity.* **125** 348-373.

[31] Berti F, Nespoli A, Villa E, Dallolio V, Passaretti F, Pennati G, Migliavacca F, Petrini L 2020 *Mater. Today Comm.* 101038.

Smart Mater. Struct. 29 (2020) 095018 (11pp) - https://doi.org/10.1088/1361-665X/aba81e

[32] Gonzalez CH, do Nascimento Oliveira CA, Cabral de Pina EA, Urtiga Filho SL, de Araújo Filho OO, de Araújo CJ 2010 *Mater. Res.* **13(3)** 325-331.

[33] Sittner P, Sedlak P, Seiner H, Sedmak P et al. 2018 *Prog. Mater. Sci.* **98** 249-298.

[34] Morgan NB, Friend CM 2001 *J. Phys. IV France* **11** 325-332.